Biochimica et Biophysica Acta 1808 (2011) 399–404

Contents lists available at ScienceDirect

Biochimica et Biophysica Acta

journal homepage: www.elsevier.com/locate/bbamem

Do main location within the cystic fibrosis transmembrane conductance regulator protein investigated by electron microscopy and gold labelling

Liang Zhang [a,1], Luba A. Aleksandrov [b], John R. Riordan [b], Robert C. Ford [a,*]

[a] Faculty of Life Sciences, The University of Manchester, MIB, 131 Princess St., Manchester M1 7DN, UK
[b] Department of Biochemistry & Biophysics, University of North Carolina, Chapel Hill, NC 27599, USA

ARTICLE INFO

Article history:
Received 12 July 2010
Received in revised form 13 August 2010
Accepted 13 August 2010
Available online 19 August 2010

Keywords:
Cystic fibrosis
Chloride channel
Structure
Electron microscopy
CFTR
Ni-NTA nanogold

ABSTRACT

The domain organisation of the cystic fibrosis transmembrane conductance regulator (CFTR) protein was studied using electron microscopy of detergent-solubilised dimeric complexes. Ni-NTA nanogold labelling data suggest that in the nonphosphorylated, nucleotide-free state, the C-terminus is intimately associated with the cytoplasmic ATP-binding regions, whilst part of the regulatory domain occupies a position close to the cytoplasmic surface of the lipid membrane. Removal of the entire second nucleotide binding domain (NBD2) results in a deficit in the CFTR structure that is consistent with the size and shape of a single NBD. The data suggest that NBD2 lies closer to the C2 symmetry axis than the first nucleotide binding domain (NBD1) and that NBD2 from one CFTR monomer also contacts NBD1 from the opposing one. These data suggest that current homology models for CFTR based on other ATP-binding cassette proteins appear to be reasonable, at least to low resolution. We also find that Ni-NTA nanogold labelling of an internal hexa-Histidine sequence is a valuable approach to locate individual protein domains.

1. Introduction

The cystic fibrosis transmembrane conductance regulator protein (CFTR, ABCC7) is a unique member of the ABC protein family that functions as a chloride channel. Deletion of amino acid residue F508, a commonly occurring mutation in CFTR leads to misfolding of the protein and a reduction of the number and activity of CFTR channels at the cell surface. Loss of CFTR function results in the lethal autosomal recessive disease cystic fibrosis [1]. CFTR contains the normal four core domains of the ABC protein plus a hydrophilic regulatory (R) region (sometimes considered to be a domain). The two core transmembrane domains (TMDs) contribute to the formation of a chloride selective pore, and the two core nucleotide binding domains (NBDs) bind and hydrolyse ATP to regulate channel gating. Phosphorylation and dephosphorylation of the R region controls channel activity [1,2]. To better understand the context of the F508del mutation within CFTR and the overall domain organisation within the protein, structural data are needed.

Structures of CFTR homologues have been published, [3–6], and structural data for isolated CFTR domains (NBD1, NBD2, R region) are available [7–9]—see the protein data bank file 3GD7 for the NBD2 structure. Expressed and purified in isolation, R region appears to have properties characteristic of a disordered polypeptide [7] and is distinct from the regulatory domains of bacterial ABC proteins [10], both in terms of primary and tertiary structure. However, it is possible that regulatory domains of ABC proteins may act in a similar fashion, by influencing the dimerisation of the NBDs [7,10,11]. Medium resolution data from 2D crystals of another member of the 'C' subclass of ABC proteins have also been recently published [12]. Low-resolution structural data from 2D crystals and single-particle analysis of the whole CFTR protein have been reported. Interestingly, isolated CFTR particles were observed to have a dimeric quaternary structure in all of the single particle averaging studies [13–15], but the 2D crystals of CFTR contained a single monomer in the unit cell [16]. Similarly, all X-ray crystal structures of ABC transporters, so far, have revealed quaternary structures equivalent to a single transporter (i.e., equivalent to a CFTR monomer) [3,6,17–21], whilst studies of noncrystalline ABC transporters by EM have reported higher levels of quaternary structure [22,23]. A recent study [15] of unstained dimeric CFTR complexes by cryo-EM and single-particle analysis revealed conformational changes induced by channel activation conditions (R region phosphorylation and ATP binding to the NBDs). The orientation of the monomers within the dimeric complex was adjudged based on the docking of the Sav1866 transporter structure [4] within the CFTR density map. This work also proposed plausible locations for the R region within CFTR based on the differences between the CFTR map and the Sav1866 homologue lacking

Abbreviations: 2D, two-dimensional; 3D, three-dimensional; CFTR, cystic fibrosis transmembrane conductance regulator; DDM, dodecyl maltoside; EM, electron microscopy; NBD, nucleotide binding domain; NTA, nitrilotriacetic acid; PAGE, polyacrylamide gel electrophoresis; SEC, size exclusion chromatography; SDS, sodium dodecylsulphate; TMD, transmembrane domain

* Corresponding author. Faculty of Life Sciences, The University of Manchester, MIB, 131 Princess St., Manchester M1 7DN, UK. Tel.: +44 1612004187.
E-mail address: bob.ford@manchester.ac.uk (R.C. Ford).
[1] Present address: Department of Cell Biology and Physiology, University of Pittsburgh, PA, 15261, USA.

0005-2736/$ – see front matter © 2010 Elsevier B.V. All rights reserved.
doi:10.1016/j.bbamem.2010.08.012

the ~200-amino acid R region [15]. Homology models for CFTR have been built on the basis of sequence alignments with the Sav1866 ABC transporter [24,25], and modelling of the R region within CFTR was attempted in one study [25].

The low-resolution structural data for CFTR were mostly consistent with the X-ray crystal structures of CFTR homologues [3–6]; however, one of the electron microscopy studies [14] reported a CFTR structure with a smooth domed surface that contained large cavities, hence implying a significantly different tertiary structure for CFTR versus other ABC proteins. Such a large change in configuration versus other ABC proteins would suggest that homology models for CFTR would need to be revised considerably and would alter our understanding of its channel properties. To resolve these discrepancies and to test the accuracy of the CFTR homology models, we describe experiments using a 1.8-nm-diameter Ni-NTA nanogold probe to label regions on the CFTR protein. We show data for labelling of an internal hexa-Histidine sequence in CFTR, as well as for the more conventional labelling of a C-terminal Histidine purification tag. These labelling data are complemented by similar studies with a truncated CFTR protein that lacks the entire NBD2 domain. Such labelling and domain removal approaches have been widely used in structural studies and have located specific sites, domains, and subunits successfully [13,26–33]. The nanogold labelling method suffers from a relatively low labelling efficiency, which may be due to a high dissociation rate of the probe [34,35], and we describe an experimental strategy to overcome this limitation to the methodology.

2. Materials and methods

2.1. CFTR expression and purification

Internal hexa-His tags were inserted into the CFTR construct with C-terminal deca-His tag at amino acids 696 and 890. A truncated CFTR construct lacking the second NBD (CFTR-X1172) was generated as described in Cui et al. [36]. The constructs were overexpressed in baby hamster kidney-21 (BHK-21) cells as described earlier [16]. Cell membranes were solubilised in dodecyl maltoside. The protein was purified according to methods described in Rosenberg et al. [16] but with a further chromatographic step using a Superdex 200 10/300 size-exclusion column [37].

2.2. Ni-NTA nanogold labelling of CFTR

CFTR protein (wild type or other constructs) and Ni-NTA nanogold (Nanoprobes Inc.) at 1:10 molar ratio were incubated together for 3 hours at room temperature. Excess Ni-NTA nanogold was removed by centrifugation at 3000 × *g* for 15 min using a 0.5-ml spin column (50 kDa cutoff) (Millipore).

2.3. Negative staining

Samples were incubated for 20 s with glow-discharged carbon-coated grids (400 mesh/in; Agar Scientific) and then blotted and transferred to a droplet of 4% (wt./vol.) uranyl acetate for 1 min before blotting dry. Grids were examined with a Philips Tecnai 10 transmission electron microscope. Images were recorded on Kodak SO-163 film or Kodak 4489 film for Ni-NTA nanogold labelled specimens, with minimal underfocus employed to optimise the imaging of the 1.8-nm-diameter gold spheres. Micrographs were developed for 1 min in full-strength Kodak D19 developer.

2.4. Image processing

Films were digitised using a UMAX PowerLook 3000 scanner. A pixel size of 3.6 Å/pixel or 4.8 Å/pixel was used. Image processing and 3D reconstruction were carried out using the EMAN software suite [38]. Single particles were interactively selected manually. The contrast transfer function (CTF) was corrected using the 'ctfit' program in the EMAN suite [38]. After correction, a high-pass filter of 1/200 $Å^{-1}$ was applied to remove low frequency information and also low-pass-filtered to a cut-off resolution of 1/20 $Å^{-1}$. After reference-free class averages were generated, the angular orientations of the characteristic views were determined using a Fourier common-lines routine [39]. A preliminary 3D density map was calculated by back-projecting the class averages [40]. Iterative refinement was carried out against the preliminary structure. Convergence was judged to be achieved when the Fourier Shell Correlation (FSC) curve between successive iterations of the refinement ceased to improve. The final 3D maps were viewed using XtalView [41] or Chimera [42]. Further details on the image processing are given in Table 1.

3. Results

3.1. Purification and homogeneity of CFTR

Various human CFTR constructs, all with a C-terminal deca-His tag were overexpressed in baby hamster kidney 21 (BHK-21) cells, and the membranes were solubilised in dodecyl maltoside according to methods described in Rosenberg et al. [16]. Subsequent purification included two steps: (i) immobilised metal (Co^{2+}-Talon) affinity chromatography with elution with 400 mM imidazole and (ii) wheat germ lectin-agarose (WGA) chromatography with elution with 0.5 M N-acetylglucosamine (GlcNAc). A relatively pure CFTR preparation was thus obtained, as judged by SDS–PAGE and Coomassie blue staining (Supplementary Fig. 1). However, electron microscopy of negatively stained specimens of the purified material (Fig. 1A), identified inhomogeneity arising from protein aggregates 20–40 nm in diameter. The majority of these aggregates appeared to be amorphous; however, in some CFTR preparations, we also observed circular aggregates ~20 nm in diameter (Fig. 1B) that appeared to have an octameric quaternary structure. Similar ring-shaped structures have been observed in preparations of the bacterial ABC transporter BmrA [22]. To improve the monodispersity of the preparations, a size exclusion chromatography (SEC) step was applied, yielding more homogeneous fields of negatively stained particles ~10 to 12 nm in diameter (Fig. 1C). A weak interaction between CFTR and the Superdex column matrix resulted in a retarded elution time, but a symmetrical peak was nevertheless observed (data not shown). Previous studies using native

Table 1
Image processing data for the data sets of negatively stained CFTR isolated in the presence of DDM.

	CFTR	Ni-NTA gold CFTR	Ni-NTA gold 696-His CFTR	Ni-NTA gold 890-His CFTR	CFTR-X1172
Calibrated pixel size at the specimen level (Å)	3.6	3.6	4.64	3.24	3.6
Box size (pixels)	64 × 64	80 × 80	48 × 48	64 × 64	64 × 64
Number of particles	4046	4412	2493	3210	2444
Mask radius (Å)	90	90	97.4	97.2	90
Final resolution cutoff (low-pass filter, $Å^{-1}$)	0.056	0.067	0.090	0.056	0.056
Resolution limit of final structure (FSC = 0.5, $Å^{-1}$)	0.048	0.050	0.038	0.043	0.048
Angle used for 3D refinement.	11.2°	11.0°	12.5°	13.8°	13.8°

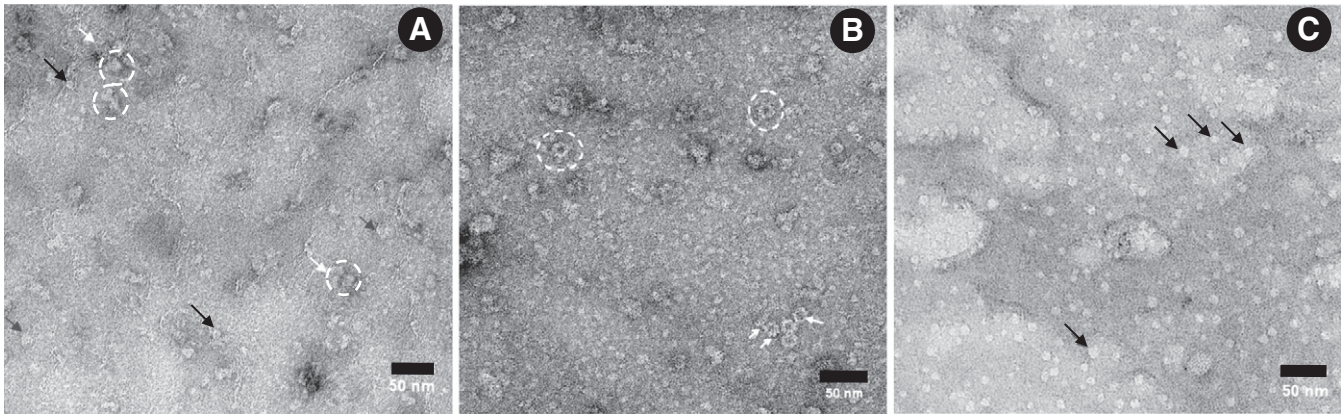

Fig. 1. (A&B) A field of CFTR particles before SEC showing (in order of abundance) 10- to 12-nm-diameter particles (black arrows), amorphous aggregates of 20–40 nm (circles, white arrows, panel A) and, in some preparations (panel B), cartwheel-shaped complexes (white arrows, circles). (C) After SEC, the 10- to 12-nm-diameter particles predominate giving a homogeneous field of stain-excluding particles (black arrows). The scale bars in each panel indicate 50 nm.

PAGE have shown that the 10- to 12-nm-diameter particles are composed of dimeric CFTR complexes that can be dissociated into monomers under various conditions [15,43–45].

3.2. Structural studies of negatively stained CFTR dimeric complexes and localization of CFTR domains

After SEC, negatively stained CFTR preparations showed uniform 10- to 12-nm-diameter particles (Fig. 1C), suggesting that single-particle image processing procedures could be applied to generate low-resolution 3D structural data for the protein [38]. Table 1 summarizes 3D structural data obtained for the various CFTR constructs studied. Three of the constructs were probed by labelling with 1.8-nm-diameter Ni-NTA nanogold spheres [30,31] before negative staining (Fig. 2A) and subsequent single-particle analysis. Removal of unbound gold particles was carried out using ultrafiltration with a 50-kDa cutoff membrane. Electron microscopy was used to confirm that the ultrafiltration step was effective (Fig. 2B). Labelling frequency was about 2–10% of the particles present, for the CFTR constructs under study. Low-frequency and variable labelling has been observed in other studies with this Ni-NTA nanogold probe [13,26–28,30,31] and is probably due to steric restriction of gold sphere binding as well as a relatively high off-rate for the probe, as reported by Lata et al. [34,35]. Labelling efficiency of 2–10% is not an insurmountable problem for the single-particle approach, since selection of labelled versus unlabelled particles is possible as the gold spheres are readily identifiable in electron micrographs. However, in the resultant data sets, selected particles display mostly a single gold sphere, introducing asymmetry into oligomeric complexes [26,27]. We therefore generated structures with C2 symmetry or no symmetry (C1) for gold-labelled CFTR. The 3D structures generated without symmetry were noisier and at lower resolution than the corresponding structures generated with C2 symmetry (Table 1); however, they were of similar size and shape, and two copies of an atomic model of an ABC protein (Sav1866) could be fitted into the low-resolution envelope of the CFTR structure, giving further justification for the application of C2 symmetry.

The low-resolution C2-symmetrised structures of CFTR are shown in Fig. 3. A comparison of full length CFTR before and after nanogold labelling is shown in Fig. 3A. Both structures are superficially similar in size and shape, especially on one side of the complex (uppermost in the panel). This upper side of the particle appears relatively featureless. However, on the opposite side of the complex, features are better defined, and there are significant differences caused by the gold labelling (yellow spheres), which is restricted to this region. The strong 'negative' density of the gold label averages over a ~3-nm-diameter region, causing deficits in the nearby protein density, which is stain-excluding and hence 'positive'. The deficits around the central position of the gold label can best be observed in the 'bottom' view in Fig. 3A. The smearing of the negative density of the gold sphere over a larger region

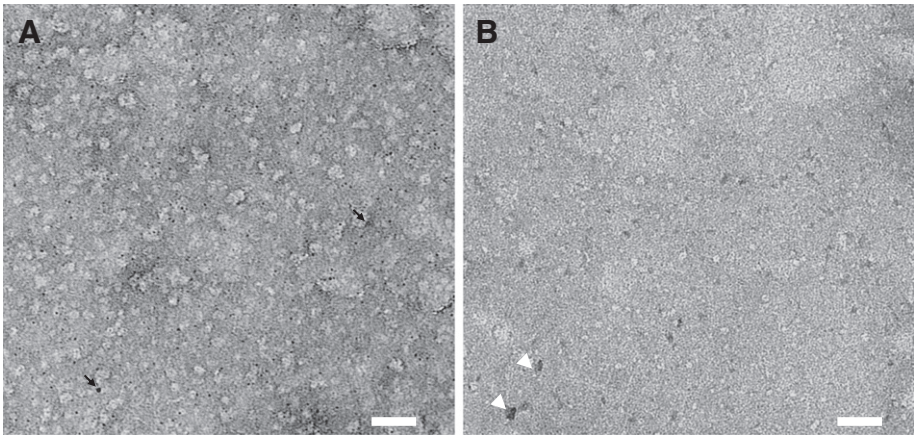

Fig. 2. (A) Electron micrograph of negatively-stained CFTR single particles labelled with 1.8 nm-diameter Ni-NTA-nanogold spheres . The gold spheres appear as small dark black dots whereas the protein particles are white. A few larger colloidal gold spheres are identifiable (arrows), but the overall size distribution of the gold spheres is relatively narrow. (B) Electron micrograph of the filtrate after filtering the Ni-NTA nanogold-labelled CFTR sample through a 50-kDa cutoff ultrafiltration device. Small stain-excluding particles can be observed as well as uncomplexed gold particles and clusters of gold spheres (arrowheads). The scale bars correspond to 50 nm.

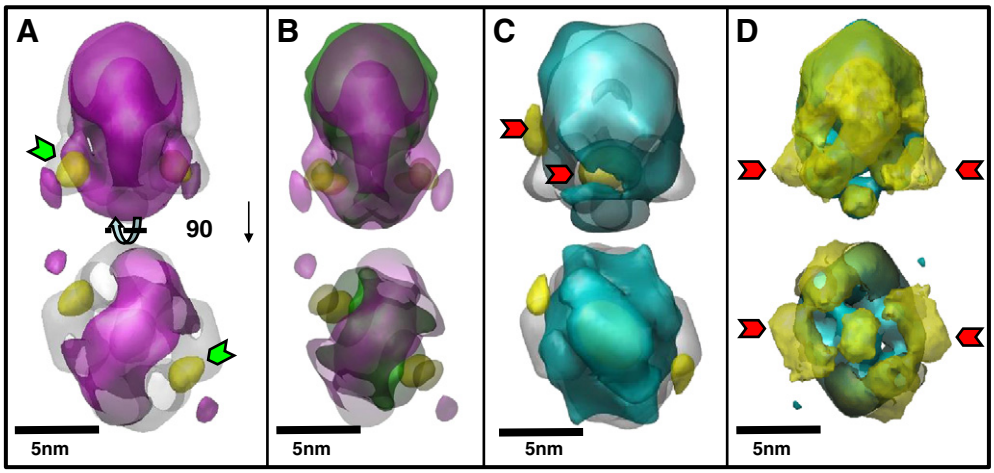

Fig. 3. 3D structures and putative location of domains in CFTR dimeric particles: (A) Comparison of CFTR (grey, transparent surface) and nanogold-labelled CFTR (purple, yellow). Top panel shows a side view. Bottom panel shows the bottom halves of the structures after a rotation as indicated. Averaged locations of the C-terminal gold labels (yellow surface, green arrows) are indicated. The strong density of the gold label, which is the opposite of the stain-excluding protein density, gives the impression of a cavity around the gold. The yellow surfaces are displayed at -10σ, grey and purple at $+2\sigma$ below/above the mean density level. (B) Comparison of nanogold-labelled CFTR (purple/yellow surfaces as in panel A) with the nanogold-labelled CFTR-890His construct (green, yellow surfaces). The gold spheres show a similar location in both structures. (C) Comparison of CFTR (grey, transparent surface) with the nanogold-labelled CFTR-696His construct (blue, yellow). Locations of the C-terminal gold label and the 696 gold label are indicated (red arrows). The yellow surfaces are at -4σ, blue and grey at $+2\sigma$. (D) Comparison of the low-resolution 3D structures of negatively stained CFTR (yellow, transparent surface) and the CFTR-X1172 construct (blue). Additional density in the putative NBD region (red arrows) is observed for the full-length CFTR structure. Some additional differences can be discerned in this view, which may be rearrangements in location of NBD1 due to the lack of NBD2 in CFTR-X1172. The surfaces are rendered at $+2\sigma$ above the mean density.

than its nominal 1.8-nm-diameter probably arises from a combination of factors: (i) some flexibility of the C-terminal His-tag, (ii) inherent spread of gold particle sizes, and (iii) lower resolution of the 3D structures (~2.5 nm) versus the size of the tag. The location of the Ni-NTA nanogold label in the lower half of the 3D structure permits its assignment as the cytoplasmic half of the particle since the C-terminus has a cytoplasmic location [46]. In comparison to the unlabelled structure, the gold sphere is intimately associated with the NBDs rather than bound on, or outside, the outer surface. This may support the idea for a functional role of the C-terminus in the C branch of the ABC family [47,48], of which CFTR is a member.

3.3. Ni-NTA nanogold labelling of internal hexa-Histidine tags in CFTR.

We also attempted to extend the gold-labelling work by inserting additional (internal) hexa-Histidine sequences into regions of CFTR adjudged to be surface-exposed and sufficiently flexible to provide a likely binding site for the Ni-NTA nanogold probes. Two constructs were generated, one with the hexa-His sequence starting at position 696 in the regulatory, R region of CFTR, the other at position 890 in the fourth extracellular loop, which also contains consensus N-glycosylation sites. These constructs were expressed and purified as before, and EM of the material after SEC demonstrated that the sample homogeneity was equivalent to the original construct of CFTR. As before, gold labelling frequency was found to be low, with a relatively small proportion of multiply labelled particles. These constructs also contained the deca-His C-terminal tag; hence, there were four potential binding sites for the Ni-NTA nanogold probe in the dimeric particles.

Labeling of the 890-His CFTR construct and structural analysis as above resulted in the generation of a 3D structure that showed well-defined gold locations, but only one gold sphere was detected per monomer corresponding to the position identified earlier as due to the C-terminal deca-His tag (Fig. 3B). This may mean that position 890 in the fourth extracellular loop is sterically occluded from the gold label, or perhaps that the local environment (e.g., nearby charged residues) could modulate the affinity of the hexa-His tag for the Ni^{2+} ion in the NTA nanogold probe. Although the labelling of the 890-His tag was unsuccessful, the reproducibility of the labelling of the C-terminal deca-His tag in this construct builds confidence in the nanogold labelling and single-particle methodology.

The 3D structure of the Nanogold-labelled 696-His CFTR construct is compared with the unlabelled CFTR structure in Fig. 3C. In this case, two sites of labelling per monomer appeared in the negative regions of the density map (red arrows, Fig. 3C). Although density at all labelling sites was somewhat smeared compared to the earlier studies, the appearance of a second site implied that this could be the averaged location of position 696 in the R region of CFTR. If this assumption is correct, then this region is close to the intracytoplasmic loops (ICLs) of the TMDs and could potentially interact with the inner surface of the plasma membrane. A previous comparison of the low-resolution structure of CFTR with a bacterial homologue lacking the R region, Sav1866 [15], shows a region of additional mass in CFTR around the surface of the NBDs and ICLs. Consistent with this hypothesis, evidence from Ni-NTA nanogold labelling suggested that the region around residue 696 in the R domain could lie near the ICLs.

3.4. Identification of NBD2

Cui et al. [36] have shown that NBD2 in CFTR can be completely removed without significant loss of expression and maturation of the protein [36]. Moreover, the truncated CFTR displays ATP-gated channel activity, albeit with altered properties compared to the full-length protein [36]. We purified and then generated a low-resolution 3D structure for the CFTR-X1172 construct lacking NBD2. This structure is shown in Fig. 3D and is compared with the structure for full-length CFTR. Although the two 3D structures are very similar on the featureless side of the complex (uppermost in Fig. 3D), on the cytoplasmic side, there are major differences, with two completely missing regions in the CFTR-X1172 structure (Fig. 3D, red arrows). We therefore expect that the missing regions correspond to NBD2 in the full-length CFTR structure, whilst the domain common to both corresponds to NBD1. To further explore this hypothesis, we generated a difference map by subtracting the CFTR-X1172 3D map from the corresponding structure for full-length CFTR. As shown in Fig. 4, the difference map shows significant positive density only on one side of the complex, with one major ellipsoidal region of density and one small peripheral density per monomer. The latter small region of density in the difference map may

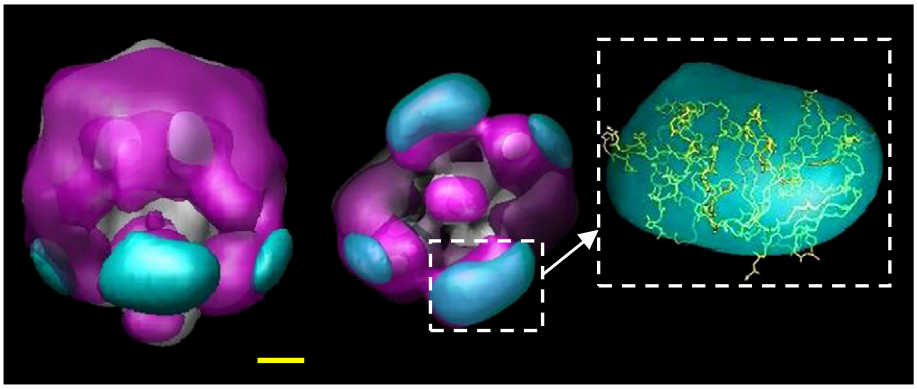

Fig. 4. (A) Side view (left) and bottom view (right) of the CFTR-X1172 construct (grey density) and the full-length CFTR (purple density) superimposed with the calculated difference map (cyan density). A large difference density can be observed (dashed box, centre). A NBD2 homology model can be automatically fitted into the difference density (zoomed region, right), although the limited resolution only allows partial orientation of the NBD model. The rest of the protein density is almost identical in the two maps at this resolution. Scale bar is equal to 20 Å.

reflect small movements in the position of NBD1 after removal of NBD2 in the CFTR-X1172 construct, but the larger ellipsoidal region directly superimposes with the position of a domain in the full-length CFTR structure. Fitting of a single NBD monomer [8] into this difference map also shows that the overall shape and dimensions of the region would match the expected envelope of NBD2 (Fig. 4, inset).

4. Discussion

In the experiments described in this article, we attempted to locate individual domains in the low-resolution 3D density maps of full-length CFTR protein. NBD2 and the C-terminus of the protein appear to be in the same (lower) half of the protein density, as expected. NBD1 is hypothesised to be the major density in this region that remains after removal of NBD2. Perhaps surprisingly, removal of NBD2 appears to have only a minor effect on the rest of the CFTR dimer. There is some evidence from these studies for a minor rearrangement in the position of NBD1, but the TMDs appear to be relatively unaffected by the truncation of the protein (Fig. 4). These structural data concur with the functional measurements on the CFTR-X1172 construct which found that the protein retained many aspects of its normal behaviour [36].

If the assignments we propose are correct, then NBD1 would seem to be the ~4-nm-diameter domain located furthest away from the twofold symmetry axis of the dimer (Figs. 3 and 4). NBD1 also appears to make more contact with NBD2 from the other molecule of the dimer rather than its cognate NBD2, which is somewhat unexpected, but may reflect an inward-facing conformation of the protein, with separation of the NBDs in each monomer. Such an arrangement has been observed in the absence of nucleotide with other ABC proteins [3,12,17,49]. Residues around amino acid 696 in CFTR lie close (within 10–20 residues) to the end of NBD1 and the start of R region [8,50]. Somewhat unexpectedly, Ni-NTA nanogold labelling of the 696 hexa-His construct indicated that the additional gold sphere was, on average, close to the intracytoplasmic loops—i.e., in a position between the TMDs and NBDs. A smeared, but nevertheless identifiable, density for the gold label assumed to bind close to the region around amino acid residue 696 in CFTR provides some evidence that the R region interacts with the rest of the protein, at least in the nonphosphorylated state. Data on isolated domains imply that phosphorylation of the R region significantly reduces its interaction with NBD1 [7].

The C-terminal tail of CFTR is an extension of 20- to 40-amino acid residues from the end of NBD2. This portion of the protein is somewhat different compared to other ABC proteins, and in CFTR, it contains a PDZ-binding consensus motif (*−DTRL*) [51–56]. The Nanogold labelling of a C-terminal deca-Histidine purification tag provided evidence that it was located on the cytoplasmic side (as expected) and roughly between the NBD1 and NBD2 domains of each CFTR monomer. Such a location implies functional significance for this region of the protein, since the formation of an NBD1–NBD2 sandwich dimer (presumably with the exclusion of the C-terminal residues) has been associated with conformational rearrangements in ABC proteins and in CFTR in particular, with activation and the opening of the chloride channel [57,58]. These observations might also suggest a way in which PDZ-binding proteins such as NHERF might influence the activity of CFTR *in vivo* [52,59].

The data presented here suggest that current homology models for CFTR [24,25,60,61] based on other ATP-binding cassette proteins appear to be reasonable, at least at a resolution sufficient to resolve the major core domains of the protein. An earlier study of negatively stained CFTR dimers, however, was not consistent with such homology models, and core domains were not resolved [14]. It is possible that the relatively hollow CFTR reconstruction generated by Mio et al. [14] was due to a combination of shallow staining (with therefore little internal detail resolved), combined with the suppression of the amplitude of low-frequency components in the images due to insufficient correction of the contrast transfer function [62].

Supplementary materials related to this article can be found online at doi:10.1016/j.bbamem.2010.08.012.

Acknowledgments

This work was supported by the Cystic Fibrosis Foundation (USA) via grants to R.C.F. and J.R.R. and by the NIH (USA) grant DK051619 to J.R.R. We thank Dr Richard Collins (University of Manchester) for electron microscopy assistance.

References

[1] D.N. Sheppard, M.J. Welsh, Structure and function of the CFTR chloride channel, Physiol. Rev. 79 (1999) S23–S45.
[2] D.N. Sheppard, M.A. Gray, X. Gong, Y. Sohma, I. Kogan, D.J. Benos, T.S. Scott-Ward, J.H. Chen, H. Li, Z. Cai, J. Gupta, C. Li, M. Ramjeesingh, B.K. Berdiev, I.I. Ismailov, C.E. Bear, T.C. Hwang, P. Linsdell, M.J. Hug, The patch-clamp and planar lipid bilayer techniques: powerful and versatile tools to investigate the CFTR Cl- channel, J. Cyst. Fibros. 3 (Suppl 2) (2004) 101–108.
[3] S.G. Aller, J. Yu, A. Ward, Y. Weng, S. Chittaboina, R. Zhuo, P.M. Harrell, Y.T. Trinh, Q. Zhang, I.L. Urbatsch, G. Chang, Structure of P-glycoprotein reveals a molecular basis for poly-specific drug binding, Science 323 (2009) 1718–1722.
[4] R.J. Dawson, K.P. Locher, Structure of a bacterial multidrug ABC transporter, Nature 443 (2006) 180–185.
[5] R.J. Dawson, K.P. Locher, Structure of the multidrug ABC transporter Sav1866 from *Staphylococcus aureus* in complex with AMP-PNP, FEBS Lett. 581 (2007) 935–938.
[6] A. Ward, C.L. Reyes, J. Yu, C.B. Roth, G. Chang, Flexibility in the ABC transporter MsbA: alternating access with a twist, Proc. Natl Acad. Sci. USA 104 (2007) 19005–19010.
[7] J.M. Baker, R.P. Hudson, V. Kanelis, W.Y. Choy, P.H. Thibodeau, P.J. Thomas, J.D. Forman-Kay, CFTR regulatory region interacts with NBD1 predominantly via multiple transient helices, Nat. Struct. Mol. Biol. 14 (2007) 738–745.

[8] H.A. Lewis, S.G. Buchanan, S.K. Burley, K. Conners, M. Dickey, M. Dorwart, R. Fowler, X. Gao, W.B. Guggino, W.A. Hendrickson, J.F. Hunt, M.C. Kearins, D. Lorimer, P.C. Maloney, K.W. Post, K.R. Rajashankar, M.E. Rutter, J.M. Sauder, S. Shriver, P.H. Thibodeau, P.J. Thomas, M. Zhang, X. Zhao, S. Emtage, Structure of nucleotide-binding domain 1 of the cystic fibrosis transmembrane conductance regulator, EMBO J. 23 (2004) 282–293.
[9] H.A. Lewis, X. Zhao, C. Wang, J.M. Sauder, I. Rooney, B.W. Noland, D. Lorimer, M.C. Kearins, K. Conners, B. Condon, P.C. Maloney, W.B. Guggino, J.F. Hunt, S. Emtage, Impact of the deltaF508 mutation in first nucleotide-binding domain of human cystic fibrosis transmembrane conductance regulator on domain folding and structure, J. Biol. Chem. 280 (2005) 1346–1353.
[10] V. Kos, R.C. Ford, The ATP-binding cassette family: a structural perspective, Cell. Mol. Life Sci. (2009).
[11] M. Mense, P. Vergani, D.M. White, G. Altberg, A.C. Nairn, D.C. Gadsby, In vivo phosphorylation of CFTR promotes formation of a nucleotide-binding domain heterodimer, EMBO J. 25 (2006) 4728–4739.
[12] M.F. Rosenberg, C.J. Oleschuk, P. Wu, Q. Mao, R.G. Deeley, S.P. Cole, R.C. Ford, Structure of a human multidrug transporter in an inward-facing conformation, J. Struct. Biol. 170 (2010) 540–547.
[13] N.H. Awayn, M.F. Rosenberg, A.B. Kamis, L.A. Aleksandrov, J.R. Riordan, R.C. Ford, Crystallographic and single-particle analyses of native- and nucleotide-bound forms of the cystic fibrosis transmembrane conductance regulator (CFTR) protein, Biochem. Soc. Trans. 33 (2005) 996–999.
[14] K. Mio, T. Ogura, M. Mio, H. Shimizu, T.C. Hwang, C. Sato, Y. Sohma, Three-dimensional reconstruction of human cystic fibrosis transmembrane conductance regulator chloride channel revealed an ellipsoidal structure with orifices beneath the putative transmembrane domain, J. Biol. Chem. 283 (2008) 30300–30310.
[15] L. Zhang, L.A. Aleksandrov, Z. Zhao, J.R. Birtley, J.R. Riordan, R.C. Ford, Architecture of the cystic fibrosis transmembrane conductance regulator protein and structural changes associated with phosphorylation and nucleotide binding, J. Struct. Biol. 167 (2009) 242–251.
[16] M.F. Rosenberg, A.B. Kamis, L.A. Aleksandrov, R.C. Ford, J.R. Riordan, Purification and crystallization of the cystic fibrosis transmembrane conductance regulator (CFTR), J. Biol. Chem. 279 (2004) 39051–39057.
[17] N.S. Kadaba, J.T. Kaiser, E. Johnson, A. Lee, D.C. Rees, The high-affinity *E. coli* methionine ABC transporter: structure and allosteric regulation, Science 321 (2008) 250–253.
[18] M.L. Oldham, D. Khare, F.A. Quiocho, A.L. Davidson, J. Chen, Crystal structure of a catalytic intermediate of the maltose transporter, Nature 450 (2007) 515–521.
[19] K.P. Locher, A.T. Lee, D.C. Rees, The *E. coli* BtuCD structure: a framework for ABC transporter architecture and mechanism, Science 296 (2002) 1091–1098.
[20] K. Hollenstein, D.C. Frei, K.P. Locher, Structure of an ABC transporter in complex with its binding protein, Nature 446 (2007) 213–216.
[21] H.W. Pinkett, A.T. Lee, P. Lum, K.P. Locher, D.C. Rees, An inward-facing conformation of a putative metal-chelate-type ABC transporter, Science 315 (2007) 373–377.
[22] M. Chami, E. Steinfels, C. Orelle, J.M. Jault, A. Di Pietro, J.L. Rigaud, S. Marco, Three-dimensional structure by cryo-electron microscopy of YvcC, an homodimeric ATP-binding cassette transporter from *Bacillus subtilis*, J. Mol. Biol. 315 (2002) 1075–1085.
[23] A. Ferreira-Pereira, S. Marco, A. Decottignies, J. Nader, A. Goffeau, J.L. Rigaud, Three-dimensional reconstruction of the *Saccharomyces cerevisiae* multidrug resistance protein Pdr5p, J. Biol. Chem. 278 (2003) 11995–11999.
[24] J.P. Mornon, P. Lehn, I. Callebaut, Atomic model of human cystic fibrosis transmembrane conductance regulator: membrane-spanning domains and coupling interfaces, Cell. Mol. Life Sci. 65 (2008) 2594–2612.
[25] A.W. Serohijos, T. Hegedus, A.A. Aleksandrov, L. He, L. Cui, N.V. Dokholyan, J.R. Riordan, Phenylalanine-508 mediates a cytoplasmic–membrane domain contact in the CFTR 3D structure crucial to assembly and channel function, Proc. Natl Acad. Sci. USA 105 (2008) 3256–3261.
[26] K. Promnares, J. Komenda, L. Bumba, J. Nebesarova, F. Vacha, M. Tichy, Cyanobacterial small chlorophyll-binding protein ScpD (HliB) is located on the periphery of photosystem II in the vicinity of PsbH and CP47 subunits, J. Biol. Chem. 281 (2006) 32705–32713.
[27] L. Bumba, M. Tichy, M. Dobakova, J. Komenda, F. Vacha, Localization of the PsbH subunit in photosystem II from the Synechocystis 6803 using the His-tagged Ni-NTA nanogold labeling, J. Struct. Biol. 152 (2005) 28–35.
[28] R.F. Collins, K. Beis, B.R. Clarke, R.C. Ford, M. Hulley, J.H. Naismith, C. Whitfield, Periplasmic protein–protein contacts in the inner membrane protein Wzc form a tetrameric complex required for the assembly of *Escherichia coli* group 1 capsules, J. Biol. Chem. 281 (2006) 2144–2150.
[29] R.F. Collins, S.A. Frye, S. Balasingham, R.C. Ford, T. Tonjum, J.P. Derrick, Interaction with type IV pili induces structural changes in the bacterial outer membrane secretin PilQ, J. Biol. Chem. 280 (2005) 18923–18930.
[30] J.F. Hainfeld, W. Liu, C.M. Halsey, P. Freimuth, R.D. Powell, Ni-NTA-gold clusters target His-tagged proteins, J. Struct. Biol. 127 (1999) 185–198.
[31] J.F. Hainfeld, R.D. Powell, New frontiers in gold labeling, J. Histochem. Cytochem. 48 (2000) 471–480.
[32] N. Nouwen, H. Stahlberg, A.P. Pugsley, A. Engel, Domain structure of secretin PulD revealed by limited proteolysis and electron microscopy, EMBO J. 19 (2000) 2229–2236.
[33] C. Buchel, E. Morris, E. Orlova, J. Barber, Localisation of the PsbH subunit in photosystem II: a new approach using labelling of His-tags with a Ni^{2+}-NTA gold cluster and single particle analysis, J. Mol. Biol. 312 (2001) 371–379.
[34] S. Lata, M. Gavutis, R. Tampe, J. Piehler, Specific and stable fluorescence labeling of histidine-tagged proteins for dissecting multi-protein complex formation, J. Am. Chem. Soc. 128 (2006) 2365–2372.
[35] S. Lata, A. Reichel, R. Brock, R. Tampe, J. Piehler, High-affinity adaptors for switchable recognition of histidine-tagged proteins, J. Am. Chem. Soc. 127 (2005) 10205–10215.
[36] L. Cui, L. Aleksandrov, X.B. Chang, Y.X. Hou, L. He, T. Hegedus, M. Gentzsch, A. Aleksandrov, W.E. Balch, J.R. Riordan, Domain interdependence in the biosynthetic assembly of CFTR, J. Mol. Biol. 365 (2007) 981–994.
[37] L. Zhang, L.A. Aleksandrov, Z. Zhao, J.R. Birtley, J.R. Riordan, R.C. Ford, Architecture of the cystic fibrosis transmembrane conductance regulator protein and structural changes associated with phosphorylation and nucleotide binding, J. Struct. Biol. (2009).
[38] S.J. Ludtke, P.R. Baldwin, W. Chiu, EMAN: semiautomated software for high-resolution single-particle reconstructions, J. Struct. Biol. 128 (1999) 82–97.
[39] M. Van Heel, Angular reconstitution: a posteriori assignment of projection directions for 3D reconstruction, Ultramicroscopy 21 (1987) 111–123.
[40] E.V. Orlova, Structural analysis of non-crystalline macromolecules: the ribosome, Acta Crystallogr. D Biol. Crystallogr. 56 (Pt 10) (2000) 1253–1258.
[41] D.E. McRee, XtalView/Xfit—a versatile program for manipulating atomic coordinates and electron density, J. Struct. Biol. 125 (1999) 156–165.
[42] E.F. Pettersen, T.D. Goddard, C.C. Huang, G.S. Couch, D.M. Greenblatt, E.C. Meng, T. E. Ferrin, UCSF chimera—a visualization system for exploratory research and analysis, J. Comput. Chem. 25 (2004) 1605–1612.
[43] M. Ramjeesingh, L.J. Huan, E. Garami, C.E. Bear, Novel method for evaluation of the oligomeric structure of membrane proteins, Biochem. J. 342 (Pt 1) (1999) 119–123.
[44] M. Ramjeesingh, J.F. Kidd, L.J. Huan, Y. Wang, C.E. Bear, Dimeric cystic fibrosis transmembrane conductance regulator exists in the plasma membrane, Biochem. J. 374 (2003) 793–797.
[45] M. Ramjeesingh, C. Li, I. Kogan, Y. Wang, L.J. Huan, C.E. Bear, A monomer is the minimum functional unit required for channel and ATPase activity of the cystic fibrosis transmembrane conductance regulator, Biochemistry 40 (2001) 10700–10706.
[46] M. Chen, J.T. Zhang, Membrane insertion, processing, and topology of cystic fibrosis transmembrane conductance regulator (CFTR) in microsomal membranes, Mol. Membr. Biol. 13 (1996) 33–40.
[47] C.J. Westlake, L. Payen, M. Gao, S.P. Cole, R.G. Deeley, Identification and characterization of functionally important elements in the multidrug resistance protein 1 COOH-terminal region, J. Biol. Chem. 279 (2004) 53571–53583.
[48] L.S. Ostedgaard, C. Randak, T. Rokhlina, P. Karp, D. Vermeer, K.J. Ashbourne Excoffon, M.J. Welsh, Effects of C-terminal deletions on cystic fibrosis transmembrane conductance regulator function in cystic fibrosis airway epithelia, Proc. Natl Acad. Sci. USA 100 (2003) 1937–1942.
[49] D. Khare, M.L. Oldham, C. Orelle, A.L. Davidson, J. Chen, Alternating access in maltose transporter mediated by rigid-body rotations, Mol. Cell 33 (2009) 528–536.
[50] J.R. Riordan, CFTR function and prospects for therapy, Annu. Rev. Biochem. 77 (2008) 701–726.
[51] K. Estell, G. Braunstein, T. Tucker, K. Varga, J.F. Collawn, L.M. Schwiebert, Plasma membrane CFTR regulates RANTES expression via its C-terminal PDZ-interacting motif, Mol. Cell. Biol. 23 (2003) 594–606.
[52] M. Favia, T. Fanelli, A. Bagorda, F. Di Sole, S.J. Reshkin, P.G. Suh, L. Guerra, V. Casavola, NHE3 inhibits PKA-dependent functional expression of CFTR by NHERF2 PDZ interactions, Biochem. Biophys. Res. Commun. 347 (2006) 452–459.
[53] P.M. Haggie, J.K. Kim, G.L. Lukacs, A.S. Verkman, Tracking of quantum dot-labeled CFTR shows near immobilization by C-terminal PDZ interactions, Mol. Biol. Cell 17 (2006) 4937–4945.
[54] M.I. Milewski, J.E. Mickle, J.K. Forrest, D.M. Stafford, B.D. Moyer, J. Cheng, W.B. Guggino, B.A. Stanton, G.R. Cutting, A PDZ-binding motif is essential but not sufficient to localize the C terminus of CFTR to the apical membrane, J. Cell Sci. 114 (2001) 719–726.
[55] B.D. Moyer, J. Denton, K.H. Karlson, D. Reynolds, S. Wang, J.E. Mickle, M. Milewski, G.R. Cutting, W.B. Guggino, M. Li, B.A. Stanton, A PDZ-interacting domain in CFTR is an apical membrane polarization signal, J. Clin. Invest. 104 (1999) 1353–1361.
[56] V. Raghuram, H. Hormuth, J.K. Foskett, A kinase-regulated mechanism controls CFTR channel gating by disrupting bivalent PDZ domain interactions, Proc. Natl Acad. Sci. USA 100 (2003) 9620–9625.
[57] D.C. Gadsby, A.C. Nairn, Control of CFTR channel gating by phosphorylation and nucleotide hydrolysis, Physiol. Rev. 79 (1999) S77–S107.
[58] D.C. Gadsby, P. Vergani, L. Csanady, The ABC protein turned chloride channel whose failure causes cystic fibrosis, Nature 440 (2006) 477–483.
[59] S. Wang, R.W. Raab, P.J. Schatz, W.B. Guggino, M. Li, Peptide binding consensus of the NHE-RF-PDZ1 domain matches the C-terminal sequence of cystic fibrosis transmembrane conductance regulator (CFTR), FEBS Lett. 427 (1998) 103–108.
[60] I. Callebaut, R. Eudes, J.P. Mornon, P. Lehn, Nucleotide-binding domains of human cystic fibrosis transmembrane conductance regulator: detailed sequence analysis and three-dimensional modeling of the heterodimer, Cell. Mol. Life Sci. 61 (2004) 230–242.
[61] S.Y. Huang, D. Bolser, H.Y. Liu, T.C. Hwang, X. Zou, Molecular modeling of the heterodimer of human CFTR's nucleotide-binding domains using a protein–protein docking approach, J. Mol. Graph. Model. 27 (2009) 822–828.
[62] R.C. Ford, A. Holzenburg, Electron crystallography of biomolecules: mysterious membranes and missing cones, Trends Biochem. Sci. 33 (2008) 38–43.